JACS
JOURNAL OF THE AMERICAN CHEMICAL SOCIETY
Article
pubs.acs.org/JACS

Charge-State Dependent Compaction and Dissociation of Protein Complexes: Insights from Ion Mobility and Molecular Dynamics

Zoe Hall,[†] Argyris Politis,[†] Matthew F. Bush,[†,‡] Lorna J. Smith,[§] and Carol V. Robinson*[,†]

[†]Department of Chemistry, University of Oxford, Physical and Theoretical Chemistry Laboratory, South Parks Road, Oxford OX1 3QZ, United Kingdom

[§]Department of Chemistry, University of Oxford, Inorganic Chemistry Laboratory, South Parks Road, Oxford OX1 3QR, United Kingdom

Supporting Information

ABSTRACT: Collapse to compact states in the gas phase, with smaller collision cross sections than calculated for their native-like structure, has been reported previously for some protein complexes although not rationalized. Here we combine experimental and theoretical studies to investigate the gas-phase structures of four multimeric protein complexes during collisional activation. Importantly, using ion mobility−mass spectrometry (IM−MS), we find that all four macromolecular complexes retain their native-like topologies at low energy. Upon increasing the collision energy, two of the four complexes adopt a more compact state. This collapse was most noticeable for pentameric serum amyloid P (SAP) which contains a large central cavity. The extent of collapse was found to be highly correlated with charge state, with the surprising observation that the lowest charge states were those which experience the greatest degree of compaction. We compared these experimental results with in vacuo molecular dynamics (MD) simulations of SAP, during which the temperature was increased. Simulations showed that low charge states of SAP exhibited compact states, corresponding to collapse of the ring, while intermediate and high charge states unfolded to more extended structures, maintaining their ring-like topology, as observed experimentally. To simulate the collision-induced dissociation (CID) of different charge states of SAP, we used MS to measure the charge state of the ejected monomer and assigned this charge to one subunit, distributing the residual charges evenly among the remaining four subunits. Under these conditions, MD simulations captured the unfolding and ejection of a single subunit for intermediate charge states of SAP. The highest charge states recapitulated the ejection of compact monomers and dimers, which we observed in CID experiments of high charge states of SAP, accessed by supercharging. This strong correlation between theory and experiment has implications for further studies as well as for understanding the process of CID and for applications to gas-phase structural biology more generally.

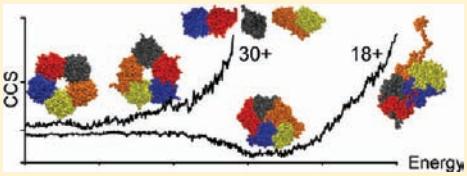

INTRODUCTION

Mass spectrometry (MS) is becoming an increasingly important adjunct to the structural biology of protein complexes. To maintain subunit interactions within the protein complex, nanoelectrospray ionization (nanoESI)−MS is employed together with various pressure regimes.[1−3] In this way, MS has been used to determine the topology and architecture of both soluble and membrane-embedded macromolecular protein assemblies.[4,5] Tandem MS, in which the protein complex undergoes gas-phase dissociation, can provide additional structural information in the form of subunit identity. Gas-phase dissociation of protein assemblies is most often achieved by subjecting the ions to high energy collisions with a gas. During CID, as the acceleration of the collisions gradually increases, the protein complex undergoes conformational changes.[6−8] Further increases in activation typically result in the unfolding of one or more monomers[9] and charge migration to the newly formed solvent-accessible regions occurs in a cooperative manner.[10] The Coulombically-driven ejection of a highly charged, unfolded monomer results,[11] leaving behind the "stripped complex". While CID of multimeric protein complexes generally results in an asymmetric partitioning with respect to mass, the partitioning of surface area (which is related to charge) is believed to be symmetric.[12] Aspects of this mechanism remain controversial,[7] in particular early conformational changes, the role of the precursor ion charge state, and the mechanism for atypical dissociation, where subcomplexes and/or compact monomers are released instead of highly charged, unfolded monomers.

Here we combine experimental and theoretical studies, using ion mobility (IM)−MS and molecular dynamics (MD) simulations, to investigate unfolding and dissociation pathways of large multisubunit protein complex ions during gas-phase activation. The complexes chosen for this study all had similar secondary structural features. This was considered important, due to the different relative gas-phase stabilities of α-helices and β-sheets.[13−15] All complexes had low α-helical content and high β-sheet content (Figure 1). While serum amyloid P component (SAP) and tryptophan RNA-binding attenuation protein (TRAP) are ring-like structures with large central cavities, avidin and transthyretin (TTR) resemble more globular

Received: October 14, 2011
Published: January 26, 2012

   dx.doi.org/10.1021/ja2096859 | J. Am. Chem. Soc. 2012, 134, 3429−3438

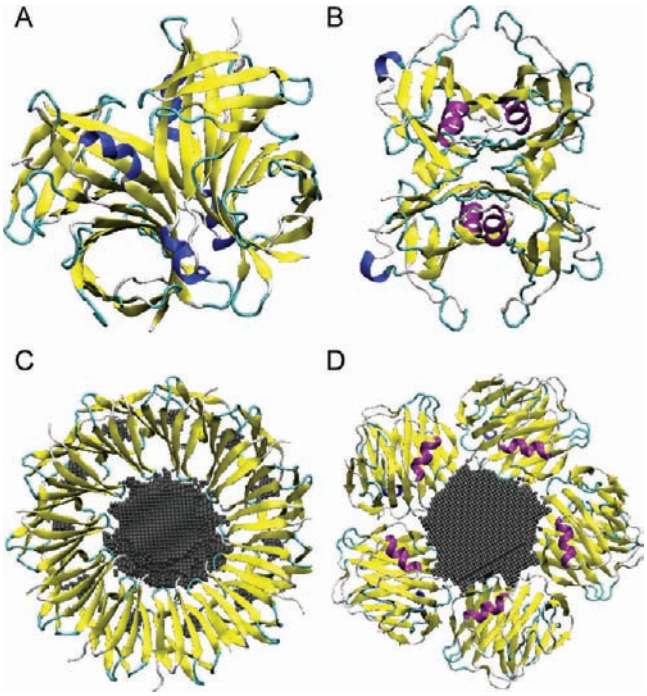

Figure 1. Structural features of protein complexes chosen for this study. The protein complexes avidin, TTR, TRAP, SAP (A through D, respectively) are colored according to their secondary structure: yellow = β-sheet, purple = α-helix, dark blue = 3_{10}-helix, light blue = loop. Internal cavities for SAP and TRAP were quantified using POCASA, and are colored gray.

compact structures, with few pockets and internal cavities. In addition, TTR and TRAP have been studied extensively,[6,9,16−18] the former with respect to dissociation mechanisms during CID and surface-induced dissociation (SID).

IM−MS provides a means by which to follow protein conformation in the gas phase.[19−21] Recently, IM−MS has provided evidence that, under appropriate conditions, native-like topologies can be maintained for protein complexes in the absence of bulk solvent.[6,22] Additional conformational stability can be conferred by ligand binding[23] and the addition of counterions.[24,25] MD is a powerful theoretical approach to study protein conformational dynamics, folding, and unfolding. Several MD studies have been carried out in vacuo, demonstrating that the major features of protein structures are preserved when transferred from solution into the gas phase.[26−31] These protein structures are thought to be kinetically trapped in near-physiological states, close to those of their X-ray crystal structures.[32] Combining such computational methods with gas-phase experiments can provide powerful insights into the structure and interactions of biomolecular ions.[33]

To address the effect of charge state on the unfolding pathways of protein complex ions, charge manipulation was carried out in solution. This was achieved using additives with high gas-phase basicity for charge reduction[17] and supercharging reagents[34] to increase the charge. For protein complexes containing a central cavity, such as SAP and TRAP, the lowest charge states were able to access more compact conformations, prior to collision-induced unfolding. By contrast, for the lowest charge states of TTR and avidin, compact conformations were not observed. MD was used to simulate the effect of collisional activation on pentameric SAP, using a linear temperature gradient to increase gradually the internal energy of the system. The unfolding of low, intermediate, and high charge states of SAP was compared in silico, and found to follow different pathways. The magnitude of compaction observed for the lowest charge states in the simulations was close to that observed experimentally using IM−MS.

Dissociation of a highly unfolded monomer was observed in simulations where the precursor ion was assigned an asymmetric charge distribution, as determined by MS of the ejected monomer. In such simulations, the collision cross section (CCS) of the dissociated monomer agreed well with experimental measurements for a monomer released from intermediate charge states of the SAP pentamer, by CID. When charge was distributed evenly among the five subunits, dissociation of compact monomers and dimers was observed. Interestingly, a shift from typical (dissociation of highly charged monomer) to atypical CID was observed experimentally for the highest charge states accessed via supercharging. CCS measurements for these dissociation products were consistent with compact monomers and dimers. Thus, the major experimental observations, including the compaction of the lowest charge states, the release of an unfolded monomer in CID of intermediate charge states, and atypical dissociation of the highest charge states, were all mirrored by MD simulations. The surprising parallel of the two approaches highlights how IM−MS, when combined with high temperature solvent-free simulations, can provide detailed insights into the gas-phase structures of macromolecular ions, as well as the conformational changes occurring during collisional activation and dissociation.

EXPERIMENTAL PROCEDURES

Preparation of Protein Complex Solutions. Human TTR and avidin from egg white were obtained from Sigma Aldrich (St. Louis, MO); human SAP was obtained from CalBioChem (Darmstadt, Germany); TRAP from *Bacillus subtilis* was a kind gift from Fred Antson (University of York, U.K.). Ammonium acetate (AA), triethylamine acetate buffer (TEA), 1, 8-diazabicycloundec-7-ene (DBU), imidazole, *m*-nitrobenzyl alcohol (*m*-NBA), and sulfolane were obtained from Sigma Aldrich (St. Louis, MO). Complex-containing solution (10 μM) was buffer exchanged into 200 mM AA buffer, pH 7.0, using Biospin-6 columns (Bio-Rad, Hemel Hempstead, U.K.). Charge reduction was carried out by the addition of TEA, DBU, or imidazole. Electrospray solutions were prepared in 200 mM AA with 10 mM (TEA, imidazole) to 20 mM (DBU) additive. Supercharging was achieved by the addition of 1% *m*-NBA or 7% sulfolane to the complex in 200 mM AA.

Ion Mobility−Mass Spectrometry Experiments. IM−MS experiments were performed on a quadrupole ion mobility time-of-flight mass spectrometer (Synapt HDMS, Waters Corp.), which had been modified such that the traveling-wave IM cell was replaced with an 18 cm drift cell with radial RF confinement (RF amplitude 200 V) and a linear voltage gradient along the axis of ion transmission.[35] In this way, CCS values can be determined directly from the slopes of drift time versus reciprocal drift voltage plots. In brief, 2 μL of complex-containing solution (~10 μM) was analyzed by nanoESI using gold-coated borosilicate capillaries prepared in-house. The following parameters were used: backing pressure 4−6 mbar, capillary voltage 1.5 kV, sample cone voltage 20 V, bias voltage 20 V, IM entrance DC 5 V, trap gas 6 mL min^{-1}, microchannel plate detector 2350 V. Helium (2.1 Torr) was used as the buffer gas, and the drift voltage varied from 50 to 200 V. The accelerating voltage into the collision cell (trap collision energy) was increased from 5 to 200 V, in 5−10 V steps. The temperature was monitored using a calibrated

dx.doi.org/10.1021/ja2096859 | J. Am. Chem. Soc. 2012, 134, 3429−3438

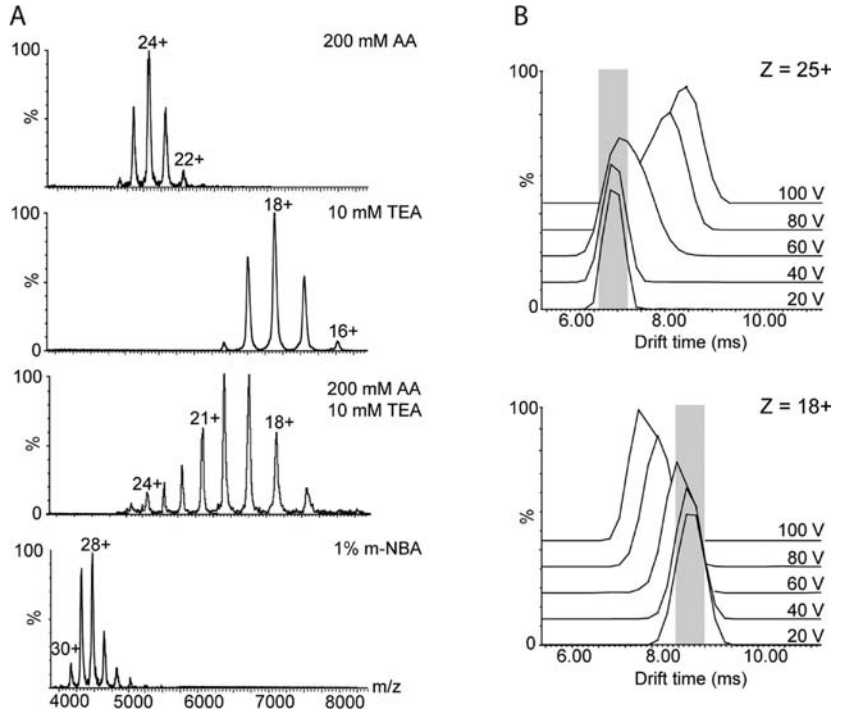

Figure 2. Charge manipulation and charge-dependent unfolding of SAP. (A) SAP 5-mer was electrosprayed from different buffer solutions in order to maximize the width of the charge state distribution (top three panels). MS spectra are shown for SAP in 200 mM ammonium acetate (AA) buffer, pH 7.0; 10 mM triethylamine (TEA) buffer pH 7.0; and a mixed buffer solution of 200 mM AA with 10 mM TEA, pH 7.0. A maximum spread of 9 charge states (17−25+) was achieved for the mixed buffer solution. Charge states 26−30+ were achieved using 1% *m*-NBA (bottom panel). (B) SAP 25+ (top) experiences an increase in drift time with increasing accelerating voltage into the collision cell. This is consistent with unfolding to more extended states. In contrast, SAP 18+ (bottom) experiences a decrease in drift time with increasing accelerating voltage, consistent with the formation of more compact states.

thermocouple (Omega Engineering Ltd.) installed directly on the outside of the IM chamber. All mass spectra were calibrated externally using a solution of cesium iodide (100 mg mL^{-1}).

X-ray Crystal Structure Calculations. Computational methods used to estimate cavity volume and interface packing density are available in the Supporting Information.

Molecular Dynamics Simulations. The simulations were run in double floating-point precision, with GROMACS[36] 4.5.3. Pentameric SAP (PDB ID 1SAC) was simulated in a solvent-free system using the OPLS-AA/L forcefield.[37] We based our simulation method on a previously published procedure[28] for simulating proteins in vacuo. A steepest descent energy minimization was performed, followed by 1 ns vacuum equilibration simulations, with randomly generated initial velocities. Initial conditions for the 10 ns vacuum simulations were taken from the final structures and velocities of the 1 ns equilibration simulations. Neither periodicity nor cut-offs were employed in the calculations, as is standard for vacuum simulations. Energy conservation was achieved using a 1 fs integration step, and constraining bonds to hydrogen with the LINCS algorithm.[38] A dielectric constant of $\varepsilon = 2\varepsilon_o$ (where ε_o is the dielectric permittivity of free space) was found to be appropriate to describe the gas-phase basicity of cytochrome c[39] and was used in our calculations. Ten nanoseconds production simulations were run over a linear temperature gradient of 300−800 K. As a control, 10 ns simulations were also performed at constant temperature (300 K). Several methods have been used to determine the protonation states for the titratable groups[40,41] of protein ions, most of which do not take into account the solvent accessibility of the residues. It is well-known that the charge states of protein ions observed during MS are highly correlated to the solvent accessible surface area.[42] Solvent accessibility is closely related to residue depth.[43] We employed a search algorithm (further details in Supporting Information) which evenly distributed a user-defined number of charges over solvent accessible basic residues (<5 Å from the surface). In this way, we assigned the charged residues for 18+, 25+, and 30+ SAP. In addition to this, we prepared six alternative configurations (two for each charge state), with charges located on different residues, including an asymmetric distribution of charges, determined from the ejected monomer in tandem MS experiments. These so-called charge isomers were used as different seeding structures for the 10 ns vacuum simulations, in order to evaluate the importance of the specific arrangement of charges. Nine trajectories, for each charge state, were analyzed with respect to their radius of gyration (R_g). In addition, CCSs were calculated for structures every 20 ps using the projection approximation (PA) method[44] implemented in MOBCAL.[45,46] The PA CCS typically underestimates experimental CCS by ∼15%.[46] For this reason, we report a scaled PA value (eq 1). This uses an empirically determined scaling factor, which accounts for scattering phenomena[47] and any missing atoms. These may occur when truncations have been carried out to the full-length protein, in order to obtain a high-resolution crystal structure of the complex.

$$\mathrm{CCS_{calc}} = 1.14\mathrm{CCS_{PA}}\left(\frac{M_{\mathrm{exp}}}{M_{\mathrm{pdb}}}\right)^{2/3} \quad (1)$$

RESULTS

Ion Mobility Experiments Reveal Collision-Induced Compaction. To access a wide range of charge states for the complexes under study, we first developed a charge reduction strategy. This was optimized on pentameric SAP. Five charge states (22−26+) were observed for SAP in ammonium acetate (AA) buffer (Figure 2A). The same protein complex in TEA buffer also had five charge states (16−20+). To maximize the width of the charge state distribution, titration of TEA concentration, in the presence of AA, was carried out. Addition

dx.doi.org/10.1021/ja2096859 | J. Am. Chem. Soc. 2012, 134, 3429−3438

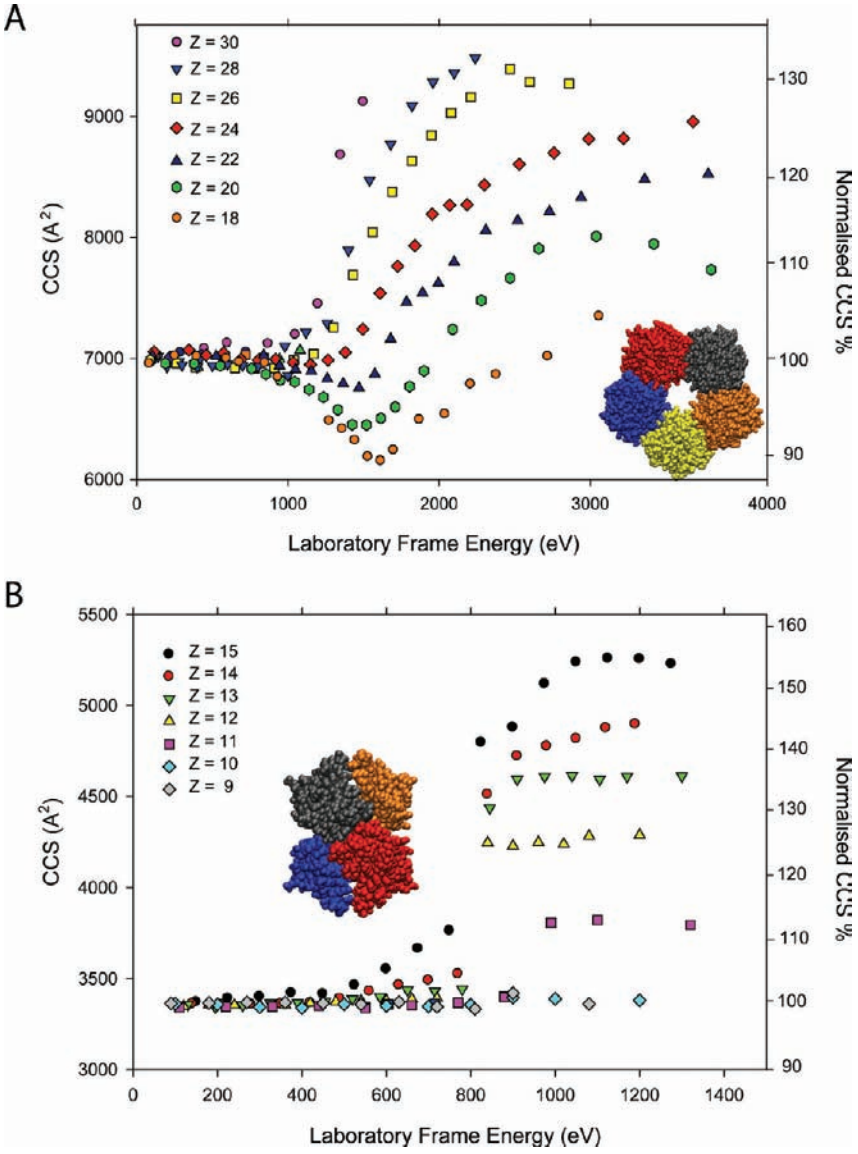

Figure 3. Unfolding pathways show dependence on charge state. The CCS of a wide range of charge states of the SAP 5-mer (A) and TTR 4-mer (B) was monitored using IM, while increasing the laboratory frame energy (accelerating voltage × charge state). Strong charge state dependence was observed for the CCS of each protein complex. For clarity, only even charge states of SAP are shown; however, the same trend was followed for the odd charge states.

of 10 mM TEA resulted in a wide charge state distribution 17−25+ (9 charge states). Higher charge states, 26−30+ were achieved by the addition of *m*-NBA or sulfolane.[48] It is not clear, however, whether such supercharging reagents affect conformation,[49,50] prompting investigation of their IM. The average CCS across all charge states, from 18+ to 30+, was 7060 Å^2, with a standard deviation ∼1%. Thus, we concluded that the gas-phase structure for SAP, at low activation energy, was highly similar across all charge states. In addition, the width and shape of the arrival time distributions recorded for each charge state of this pentameric assembly indicated the presence of one major conformation, or one ensemble of closely related conformations, thus, validating our charge manipulation approaches.

The next step was to examine the various charge states of SAP and their response to activation. By increasing the accelerating voltage into the collision cell, we can control the amount of collisional activation. As the collision energy is raised, this results in the transfer of increased amounts of kinetic energy to the biomolecular ions. At a defined accelerating voltage, ions with the highest charge states undergo increased energetic collisions with the collision gas (argon). For this reason, we define activation energy using the term laboratory frame energy E_{lab}, which takes into account the charge state, Z of the ion (eq 2).

$$E_{lab} = \text{Accelerating voltage} \times Z \quad (2)$$

Arrival time distributions are shown for two charge states of SAP (Z = 25+ and Z = 18+) (Figure 2B). From 20 to 100 V, the drift time for SAP 25+ can be seen to increase dramatically, corresponding to ions populating increasingly extended states. This is consistent with collisional unfolding.[7] Surprisingly, a decrease in drift time was observed for the SAP 18+ charge state as the accelerating voltage was increased. This significant shift in drift time indicated conformational changes consistent with compaction. A plot of laboratory frame energy against

dx.doi.org/10.1021/ja2096859 | J. Am. Chem. Soc. 2012, 134, 3429−3438

CCS for charge states 18−30+ of SAP revealed a general decrease in CCS prior to a large increase (Figure 3A). We interpret this as the formation of a more compact state than the native-like structure, prior to unfolding into more extended conformers. Interestingly the degree of compaction before unfolding was greatest for the lowest charge states. At the lowest activation energy, the CCS for the 18+ ion of SAP was 6900 Å^2. This decreased to a minimum CCS of 6200 Å^2 at E_{lab} of 1620 eV, corresponding to ∼10% compaction. The CCS for SAP 22+ decreased from 7020 Å^2 at low activation energy to a minimum of 6760 Å^2 (4% compaction) at E_{lab} of 1480 eV. The highest charge states (25+ to 30+) did not show any CCS decrease but rather at E_{lab} > 1000 eV began to increase due to collisional unfolding. Overall therefore, these results demonstrate a clear compaction of the lowest charge states of the SAP pentamer, one that is unexpected given the precedence for compaction of higher charge states reported previously.[6]

To determine whether this charge-state dependent compaction was specific to SAP or could be observed for other protein complexes, we measured CCSs of three additional protein complexes (TTR, TRAP, and avidin) and compared these with the results obtained for SAP. We used the same mixed buffer approach to generate a broad charge state distribution and increased the activation energy incrementally. In this way, a similar trend to SAP was obtained for TRAP (Figure S1A). A 4% decrease in CCS was observed prior to unfolding for the lowest charge state generated (14+). This compaction was less significant as the charge state increased from 14+ to 17+, until 19+ when unfolding proceeded with no prior compaction. We conclude that, similar to SAP, TRAP undergoes compaction of the lowest charge states. Interestingly the extent of compaction measured is less for TRAP than for SAP.

Turning our attention to TTR, the average CCS for the charge states 9+ to 15+ was 3370 Å^2, at the lowest activating conditions, with <1% standard deviation between all charge states (Figure 3B). As the E_{lab} was raised, higher CCSs were observed consistent with the ions populating increasingly extended populations. No compaction was observed for any of the charge states investigated. While at low energy there was no difference between CCS of different charge states, at higher activation energies, the CCS increased with escalating charge state. For example, at E_{lab} 1000 eV, the CCSs for TTR 11+, 13+, and 15+ were 3820, 4610, and, 5170 Å^2, respectively. The addition of 20 mM DBU, which has higher gas-phase basicity than TEA, was carried out in order to access further lower charge states for TTR. In this way, CCSs measured at E_{lab} 1000 eV for TTR 9+ and 10+ were 3370 and 3380 Å^2. These values were similar to CCS measurements taken at the lowest E_{lab} values. TTR 10+ and 9+ did not experience unfolding, even under the maximum accelerating voltages accessible. Similar results were obtained for avidin (Figure S1B), which did not show evidence for a compact conformation. As with TTR, the lowest charge state for avidin (10+) did not undergo unfolding, or compaction, even at maximum activation energies.

To assess whether the additive itself influenced the gas-phase unfolding of ions, aside from affecting the charge state, the CCS of SAP 22+ was monitored during activation, following electrospray from a variety of solution conditions. No differences in the unfolding pathways of the 22+ ions were observed in AA, AA with 10 mM TEA, or AA with 10 mM imidazole. In all cases, compaction, followed by unfolding, was observed (Figure S2A). Similarly the addition of 10 mM TEA, 20 mM DBU, or 10 mM imidazole had no effect on the unfolding pathway of avidin 13+ (Figure S2B). Thus, we conclude that the solution additives themselves do not affect unfolding but rather the charge state of the ion is the critical factor. Furthermore, the drift times were monitored for SAP in negative ion mode during collisional activation (Figure S3). Interestingly, an initial decrease in drift time was observed, consistent with compaction, as was observed for the experiments performed in positive ion mode. This was followed by an increase in drift time at higher collision energies, consistent with unfolding. The agreement between the two ion modes indicate that both the conformation and the gas-phase behavior during collisional activation are the same for SAP pentamer, regardless of whether it has an excess of positive or negative charges.

Molecular Dynamics Simulations Corroborate Experimental Results. Although MD has been used previously to examine proteins, peptides, and even small complexes, it is not clear how these methods would recapitulate macromolecular complexes in the gas phase, particularly during activation. To investigate this, we first examined the MD trajectories for SAP 18+ under vacuum. The radius of gyration (R_g) for SAP 18+ was computed along the trajectories and was found to be constant over the 10 ns simulation at 300 K (Figure S4A). In contrast, during the 10 ns simulation of SAP 18+ with increasing temperature (300−800 K) (Figure 4), large conformational changes were evident. From analysis of R_g, we have divided the simulation into three phases (Figure S5A). In the first phase (0−3 ns), at lower temperatures, there is little

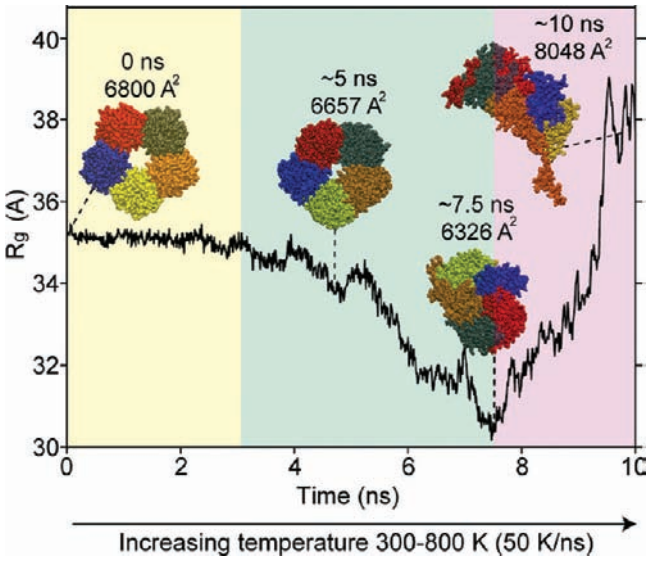

Figure 4. In vacuo molecular dynamics simulations of SAP 18+. Radius of gyration for SAP over 10 ns simulation with a linear temperature gradient (300−800 K), in order to represent increasing activation energy during collisional activation in IM−MS experiments. A representative trajectory is shown for SAP 18+, with charges evenly distributed over the surface-accessible basic residues. Additional trajectories are shown in Figure S5. An RMSD-based clustering analysis was performed to identify the most populated conformational states during different stages of the trajectory (see Supporting Information). These illustrate the native-like ring topology (0−3 ns, yellow) becoming distorted into a buckled ring, followed by collapse of the ring (3−7.5 ns, green). Finally, significant unfolding, consistent with the extension of a monomer was observed (7.5−10 ns, purple). CCSs were calculated for these structures.

dx.doi.org/10.1021/ja2096859 | J. Am. Chem. Soc. 2012, 134, 3429−3438

change in R_g, indicating the initial ring-like structure is retained. This is followed by a decrease in R_g (3−7.5 ns) of up to 15%. The final phase of the simulation (7.5−10 ns) is marked by an increase in R_g, to ∼10% above its initial value. Coordinates were extracted from a representative trajectory, and their CCS calculated, in order to observe the conformational changes to the assembly. RMSD-based clustering was used to identify the most populated conformations at different stages in the trajectory (Figure S5B). Representative structures at different time points were thus compared to the structure at 0 ns, which corresponded to the initial native-like ring topology (CCS_{calc} 6800 Å^2). The R_g decrease was associated with the symmetrical ring topology distorting into a buckled ring (∼5 ns, CCS_{calc} 6657 Å^2), gradually becoming more collapsed, reaching a minimum value at ∼7.5 ns (CCS_{calc} 6326 Å^2). The CCS of the smallest conformation was thus 7% lower than the CCS at 0 ns. The subsequent increase in R_g after 8 ns is due to considerable conformational change, consistent with the extension of one or more monomers (∼10 ns, CCS_{calc} 8048 Å^2).

Effect of Charge State on Compaction and Unfolding in Silico. Having established simulation conditions for SAP 18+, the effect of charge state on the conformational changes observed was investigated by carrying out simulations for two additional charge states of SAP (25+ and 30+). From IM−MS experiments, SAP 18+ and 25+ were selected to represent low (charge-reduced) and intermediate charge states, respectively. SAP 30+ was chosen for MD simulations to reflect a supercharged state. In addition, in order to evaluate the importance of the specific arrangement of charges on the in silico unfolding pathway, two additional charge configurations, including an asymmetric arrangement, were prepared for each of the three charge states investigated. Analysis of 9 trajectories, for each charge state, was conducted. Different charge configurations were investigated for each charge state. There was relatively low variability in the extent of compaction observed for these different charge configurations (Table S1). In contrast, distinct pathways could be observed when the overall charge states were different (18+, 25+, 30+) (Figure 5). The lowest charge state (Z = 18+) experienced the greatest decrease in CCS (ΔCCS_{calc} −7%) before unfolding with a corresponding increase in CCS. The average CCS decrease for the intermediate charge state (Z = 25+) was 3%. The highest charge state (Z = 30+) did not undergo any significant decrease in CCS, only a rapid increase in CCS after 4 ns. These results clearly show that, despite different arrangements of the charges on the protein complexes, it is the overall charge state value that is the key determinant of collapse for a protein complex with an internal cavity.

Insights into Collision-Induced Dissociation. In our MD simulations, the charges are fixed and cannot migrate to newly exposed surface area, occurring as a result of unfolding. Therefore, in order to simulate CID in silico, we carried out simulations on the 25+ charge state of SAP, with an asymmetric distribution of charges. CID was carried out experimentally on the SAP 5-mer 25+ ion by MS/MS, and the average charge state of the dissociated monomer was determined experimentally as 11.7+. Twelve charges were therefore distributed evenly over the surface-accessible basic residues of one monomer in its compact state, with the remaining 13 charges distributed over the accessible basic sites of the remaining four monomers. Simulations were carried out as described previously. After ∼9 ns, dissociation of a highly charged monomer was observed. The CCS of the monomer gradually increased over the course

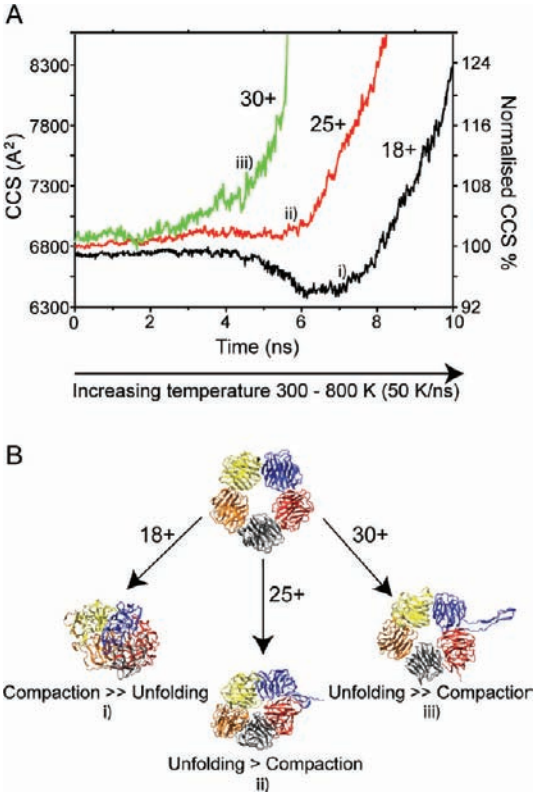

Figure 5. Effect of charge state on unfolding pathways in silico. (A) CCSs were calculated for SAP over 10 ns MD simulations with a linear temperature gradient (300−800 K). Average values for all trajectories are shown in green, red, and black for three different charge states of SAP: 30+, 25+, and 18+, respectively. (B) During the high temperature simulations, SAP 18+ collapsed to compact conformational states, prior to unfolding. SAP 25+ compacted to a lesser extent than 18+, with a greater degree of unfolding. SAP 30+ proceeded to unfold, with no prior compaction. The structures shown are the most populated conformations (based on RMSD-clustering) in the regions (i−iii), from a representative trajectory.

of the simulation (Figure 6), corresponding to progressive loss of structure. The average CCS of the newly dissociated monomer was ∼3500 Å^2, significantly greater than the bound monomer (CCS_{calc} 1990 Å^2) in the native-like structure at 0 ns. This shows close agreement to the experimental CCS of one dissociated monomer, which was measured to be 3200 Å^2 (12+). In contrast, MD simulations revealed that the tetramer, which remains intact after dissociation of the monomer, did not undergo significant changes in CCS, increasing just 5% from its initial value of 5870 Å^2.

During CID experiments of the supercharged SAP 30+, the dissociation of monomers (25.5 kDa) and dimers (51.0 kDa) was observed. The average charge state of the monomer (6+) indicated a significantly different structure to the monomer (12+) released during CID of SAP 25+ above. Experimental CCS were measured and found to be consistent with CID pathways resulting in the dissociation of compact monomers (1880 Å^2) and compact dimers (3760 Å^2). This was reproduced using either *m*-NBA or sulfolane as the supercharging reagent. Interestingly, during MD simulations of SAP 30+, where each subunit carried an equal number of charges (6+), the dissociation of compact dimers (CCS_{calc} 3795 Å^2) and monomers (CCS_{calc} 2220 Å^2) was observed, in line with experimental observations. By following the backbone RMSD

dx.doi.org/10.1021/ja2096859 | J. Am. Chem. Soc. 2012, 134, 3429−3438

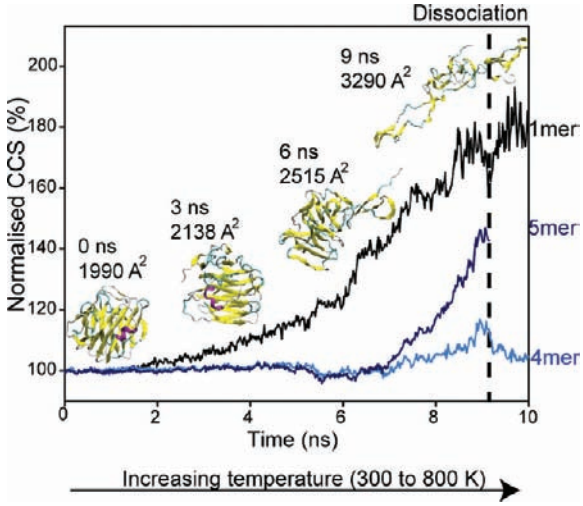

Figure 6. Collision-induced dissociation of SAP 25+. MD simulations of SAP 5-mer (25+), with a linear temperature gradient (300−800 K) were run. The precursor ion had charges asymmetrically distributed; one subunit had 12+ (as determined by MS/MS), one 4+, and the remaining three subunits each had 3+. The average CCS was monitored for SAP monomer (12+), 4-mer (13+), and intact complex (black, light blue, dark blue, respectively). Prior to dissociation, monomer and 4-mer coordinates were extracted from the intact complex to calculate CCS. RMSD clustering was carried out and representative structures at different stages in one trajectory, for the monomer, are shown at 0, 3, 6, and 9 ns along with their CCS.

of individual subunits, relative to the starting structure at 0 ns, distinct pathways for unfolding and dissociation can be clearly seen for the 25+ and 30+ charge states of SAP (Figure 7) during simulations.

In contrast, MS/MS experiments on SAP 18+ (Figure 7B) resulted in the majority of the precursor ions remaining intact, even at the highest collision energies accessible. A very small population of dissociated monomer was observed, with charge state centered on 9+. Thus, in order to simulate CID of SAP 18+, 9 charges were distributed evenly over the surface-accessible basic residues of one monomer, with an additional 9 charges distributed over the accessible basic sites of the remaining four monomers. During the simulations, SAP 18+ underwent conformational changes consistent with compaction and unfolding, as described above; however, no dissociation was observed. The fact that all simulations of the three different charge states of the complex recapitulate our experimental observations is remarkable given the size and complexity of the macromolecular ions investigated and the limited understanding of the effects of gas-phase activation on 3D structure.

DISCUSSION

One of the major limitations of MD is its inability to match the time scale over which the protein undergoes structural rearrangements (often >1 ms). The computational cost of running all-atom calculations for these time scales makes such simulations impractical. One way to overcome this is to run simulations at elevated temperatures. This approach is commonly used to study protein unfolding in bulk-solvent.[15,51,52] Elevated temperature simulations, including simulated annealing and replica-exchange molecular dynamics (REMD), have also been applied to in vacuo studies to allow enhanced sampling[53,54] and to correlate CCS data, from IM−MS, with candidate structures.[55] We chose a linear temperature gradient for our in vacuo MD simulations, in order to impart increasing amounts of energy to the system, to mimic IM−MS activation experiments. This gradient was also chosen to enhance sampling, such that simulations could be carried out over reasonable time scales. A further important consideration for the simulations is the choice of charge distribution. In our study, we differentiate between "symmetric" and "asymmetric" distributions. In reality, the arrangement of charges is unlikely to be perfectly symmetrical. Local areas of slightly higher charge density are thought to play a role in triggering unfolding, which in turn prompts charge migration to maintain a uniform surface charge density.[7] Charge migration is not yet possible in our simulations, and therefore, the use of fixed charges and the choice of charge distribution reflects one of the limitations of the theoretical model. While it is difficult to know precisely what happens to protein complexes in the gas phase, key steps observed in IM−MS experiments were captured in MD simulations, where experimentally determined charge states were used.

1. Observation of a Compact State Prior to Unfolding in a Cavity-Containing Complex. The collapse of ring-like structures in the gas phase has been documented previously. For instance, complexes whose subunits are arranged in ring-like architectures have been shown to undergo significant collapse upon dissociation in the gas phase.[56] In addition, an early IM−MS study[6] showed higher charge states of TRAP to be more compact. This was carried out on a prototype instrument, using a higher energy regime than used in our study. However, our IM−MS experiments reveal the lower charge states of SAP and TRAP passed through an intermediate compact state, prior to unfolding. Both SAP and TRAP complexes had cavities calculated to be ∼7% of their total volumes. The lowest charge states of these complexes exhibited a decrease in experimental CCS of 10% (SAP) and 4% (TRAP). Thus, SAP experienced CCS decrease 3% greater, and TRAP 3% less, than expected from the size of the cavity alone. Since the CCS decrease does not correlate solely with cavity size, an assessment of the interface packing density was carried out for the two protein complexes using the gap volume packing index.[57] The gap volume index corresponds to the volume of interface cavities, normalized with respect to the buried surface area.[58] Here, an interface cavity is defined as a packing defect in protein tertiary structure, which can accommodate a probe of a defined size.[59] Typical values for protein complexes are 2.5 ± 1.0 Å.[60] The gap volume indices for TRAP and SAP were calculated; TRAP had a gap volume index of 0.99 Å, indicating that subunits are twice as well packed as those in SAP (gap volume index 2.32 Å). Consequently, for a structure with high interface packing density, where subunit interactions are more rigid, less compaction is observed than would be anticipated for a totally collapsed structure. This, therefore, could account for the differences observed for these two complexes between the cavity size and degree of compaction during collisional activation.

2. Lowest Charge States Experience the Greatest Degree of Compaction. We investigated the charge-state dependence of the compaction observed for cavity-containing proteins. The ability to modulate charge state without affecting conformation was critical for this. To access a wide range of charge states for the complexes, we employed a charge reduction strategy based on the addition of TEA to AA buffer.[61,62] Charge reduction was attributed to the fact that

dx.doi.org/10.1021/ja2096859 | J. Am. Chem. Soc. 2012, 134, 3429−3438

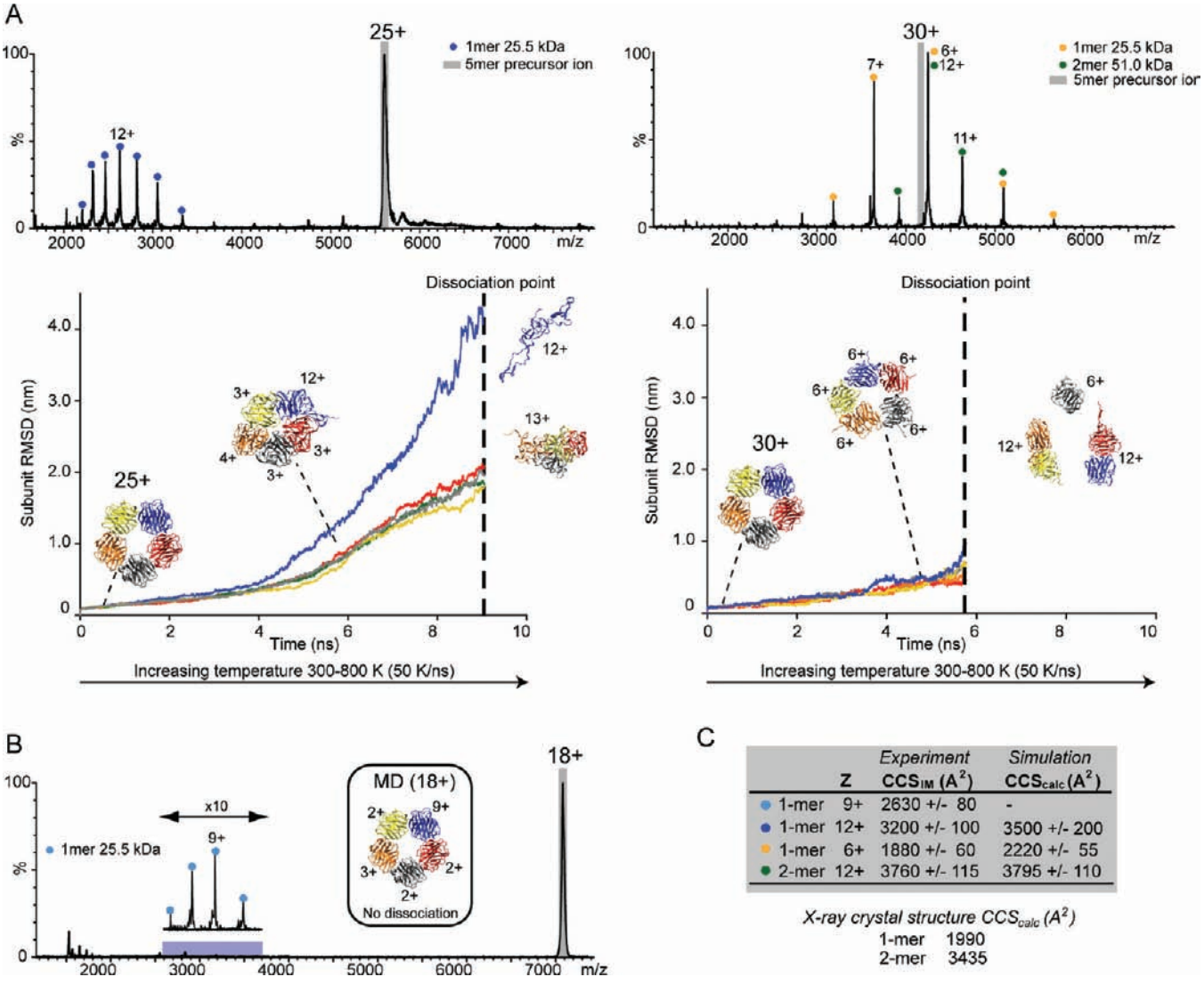

Figure 7. Charge-dependent dissociation pathways for SAP. (A) MS/MS spectra for SAP 25+ and 30+ are shown. CID of SAP 25+ results in loss of a highly charged monomer, while SAP 30+ releases dimers, and less highly charged monomers. The average charge states observed for CID products were used to assign the charge distributions in MD simulations. Thus SAP 25+ had charges asymmetrically distributed, with one subunit carrying 12+, and the remaining 13+ evenly distributed over the other four subunits. For SAP 30+, each subunit had 6+. The backbone RMSD of individual subunits locally superimposed, from the starting structure at 0 ns, was monitored during simulations, and an average for all the equivalent trajectories is shown. For SAP 25+, the highly charged monomer exhibited more extensive conformational changes than the other four subunits, prior to the dissociation of an extended monomer at ~9 ns. For SAP 30+, each subunit underwent a similar degree of conformational change (significantly lower than that for SAP 25+), before dissociation of compact monomers and dimers at ~6 ns. Representative structures are shown at different time points, for one trajectory each, during simulations of SAP 25+ and 30+. (B) MS/MS spectrum for SAP 18+, indicating very little dissociation of the precursor ion. A small population of monomer, with charge state centered on 9+, can be observed in the inset (×10). No dissociation was observed in MD simulations of SAP 18+, with one monomer carrying 9+. (C) The CCS of dissociation products from MD and measured using IM−MS following CID experiments.

TEA has higher gas-phase basicity (951 kJ mol^{-1}) than AA (819 kJ mol^{-1}). The gas-phase basicity of the ionic species present in the electrospray droplet governs how much charge is emitted from the droplet. Small ionic species present in the droplet can be emitted, carrying with them an associated charge, effectively competing for charges with ionized sites of the protein. Electrolytes with higher gas-phase basicities will therefore remove more charge from the protein.[63,64] In IM−MS experiments with activation, a relationship was observed between decreasing charge state and the extent of compaction for SAP and TRAP. This trend was mirrored by the MD simulations, where SAP 18+ showed a greater degree of compaction than equivalent simulations of SAP 25+ and 30+. It seems likely that by reducing the charge, the energy barrier to unfolding is increased, and thus, more energy is required in order to initiate unfolding.[65] At low charge states, compact states become increasingly accessible upon sufficient activation to overcome the barrier for collapse.

3. Less Energy Is Required To Unfold Higher Charge States. This is supported by both our experimental observations and simulations, wherein higher charge states required less energy to initiate unfolding. A clear relationship between charge state and the extent of unfolding was demonstrated by IM−MS for all the complexes studied, with higher charge states able to access more highly extended conformations than lower charge states. This is in agreement

dx.doi.org/10.1021/ja2096859 | J. Am. Chem. Soc. 2012, 134, 3429−3438

with early theoretical and experimental studies, which noted that higher charge states of monomeric proteins, lysozyme and cytochrome c, were more prone to unfolding in vacuo.[39,66] Interestingly, the lowest charge states of avidin and TTR did not unfold, even at maximum activation energies accessible. One explanation for this observation is that unfolding competes with dissociation.[10,65] For the lowest charge states of avidin and TTR, the energy barrier for unfolding is increased, such that the energy required for dissociation is lower than that for unfolding. This is consistent with a previous study[17] which showed that lower charge states of TTR, which had been charge-reduced using crown ethers, ejected folded, rather than extended, monomers during CID.

4. Loss of an Unfolded Monomer Occurs from Asymmetrically Charged Complex Ions. Alternative CID pathways, which do not result in monomer dissociation, have been described for a few protein complexes.[67,68] The detailed mechanism by which this unusual form of dissociation occurs is not fully understood, but is thought to be affected by the strength of intermolecular interactions and the overall charge density. Dissociation of intact charge-symmetric subcomplexes has also been reported during SID,[69,70] where dissociation occurs on a faster time scale than unfolding due to the rapid high energy deposition. In our simulations of SAP 25+, where one subunit carried approximately half the number of total charges, the dissociation of a highly unfolded monomer was recapitulated. It is important to note that dissociation of an extended monomer, in MD simulations, only occurred from precursor ions with asymmetric charge state configurations. Equivalent simulations, with charges evenly distributed over the pentameric assembly, resulted in the dissociation of compact monomers and dimers. This form of dissociation was observed during CID experiments of the highest charge states of SAP, accessed by supercharging. A gradual shift from typical to atypical dissociation was observed experimentally as the charge state of the precursor ion increased from 18 to 30+ (Figure S6). One explanation for the atypical CID pathway observed for the highest charge states of SAP is that the energetic gap between dissociation and unfolding becomes reduced by charge repulsion, allowing dissociation to occur without the need for prior unfolding.[68] An alternative explanation is that increased amounts of internal energy are deposited during CID for the highest charge states, which are accelerated to a greater degree than lower charge states. This could result in dissociation occurring on a shorter time scale than structural rearrangement. Whatever the origin of this dissociation, its observation prompts further investigation, particularly as it may yield heterodimers and trimers from heteromeric assemblies.

CONCLUSION

IM−MS experiments were carried out on protein complexes with similar secondary structure, but differing in their internal cavities. All the complexes studied maintained their native-like structures in the gas phase at lower energies. This is a very important finding since it is a vital requirement for the incorporation of IM−MS in current and future structural biology approaches. During collision activation, complexes with large internal cavities, such as SAP and TRAP, could access significantly more compact conformations. The degree of compaction was also found to be strongly charge-state dependent. The lowest charge states are able to access highly compact conformations, with up to 10% lower CCS than the native-like structure. The lowest charge states are thought to be able to access compact conformations upon sufficient activation, due to an increased energy barrier for unfolding. As the charge state increases, unfolding progresses without passing through an intermediate compact state. In addition, the dissociation pathway shifts from typical, with the loss of an extended monomer, to atypical, where the loss of compact monomers and dimers was observed for supercharged SAP.

Relative changes in CCS during IM−MS activation experiments for SAP were also closely reflected in MD simulations, which were carried out in vacuo, and under conditions of increasing temperature. During simulations in which the precursor ion had one monomer carrying a higher number of charges than the remaining four subunits, the loss of a highly unfolded monomer was recapitulated. Equivalent simulations where each subunit carried an equal number of charges resulted in the dissociation of compact monomers and dimers, as observed experimentally. Overall, this study highlights the potential of high temperature vacuum MD simulations of complexes, in combination with experimental data from IM−MS and CID, to provide additional insights into the processes of rearrangement, unfolding, and dissociation. In addition, the ability to control the outcome of CID, by charge manipulation, to release intact subcomplexes has great potential in gas-phase structural biology.

ASSOCIATED CONTENT

Supporting Information

Supplementary experimental procedures, Table S1, Figures S1−S6, as mentioned in text. This material is available free of charge via the Internet at http://pubs.acs.org.

AUTHOR INFORMATION

Corresponding Author

carol.robinson@chem.ox.ac.uk

Present Address

‡Department of Chemistry, University of Washington, Seattle, Washington 98195, United States

Notes

The authors declare no competing financial interest.

ACKNOWLEDGMENTS

The authors thank Cesar Tron-Lozai, Mark Sansom, Sarah Rouse (all from University of Oxford); Mark Thachuk, Sarah Fegan (both from University of British Columbia) and Erik Marklund (University of Uppsala) for useful discussions. Justin L. P. Benesch (University of Oxford) is acknowledged for critical reading of the manuscript. This work was funded by an ERC Advanced Grant. C.V.R is a Royal Society Professor.

REFERENCES

(1) Benesch, J. L.; Ruotolo, B. T.; Simmons, D. A.; Robinson, C. V. *Chem. Rev.* **2007**, *107*, 3544.
(2) Sobott, F.; Hernández, H.; McCammon, M. G.; Tito, M. A.; Robinson, C. V. *Anal. Chem.* **2002**, *74*, 1402.
(3) Hernández, H.; Robinson, C. V. *Nat. Protoc.* **2007**, *2*, 715.
(4) Zhou, M.; Morgner, N.; Barrera, N. P.; Politis, A.; Isaacson, S. C.; Matak-Vinkovic, D.; Murata, T.; Bernal, R. A.; Stock, D.; Robinson, C. V. *Science* **2011**, *334*, 380.
(5) Uetrecht, C.; Barbu, I. M.; Shoemaker, G. K.; van Duijn, E.; Heck, A. J. R. *Nat. Chem.* **2011**, *3*, 126.
(6) Ruotolo, B. T.; Giles, K.; Campuzano, I.; Sandercock, A. M.; Bateman, R. H.; Robinson, C. V. *Science* **2005**, *310*, 1658.
(7) Benesch, J. L. P. *J. Am. Soc. Mass Spectrom.* **2009**, *20*, 341.

(8) Michaelevski, I.; Eisenstein, M.; Sharon, M. *Anal. Chem.* **2010**, *82*, 9484.
(9) Ruotolo, B. T.; Hyung, S. J.; Robinson, P. M.; Giles, K.; Bateman, R. H.; Robinson, C. V. *Angew. Chem., Int. Ed.* **2007**, *46*, 8001.
(10) Wanasundara, S. N.; Thachuk, M. *J. Am. Soc. Mass Spectrom.* **2007**, *18*, 2242.
(11) Jurchen, J. C.; Williams, E. R. *J. Am. Chem. Soc.* **2003**, *125*, 2817.
(12) Benesch, J. L.; Aquilina, A.; Ruotolo, B. T.; Sobott, F.; Robinson, C. V. *Chem. Biol.* **2006**, *13*, 597.
(13) Vijayakumar, S.; Vishveshwara, S.; Ravishanker, G.; Beveridge, D. L. *Biophys. J.* **1993**, *65*, 2304.
(14) Benson, N. C.; Daggett, V. *Protein Sci.* **2008**, *17*, 2038.
(15) Daggett, V. *Acc. Chem. Res.* **2002**, *35*, 422.
(16) Sobott, F.; McCammon, M. G.; Robinson, C. V. *Int. J. Mass Spectrom.* **2003**, *230*, 193.
(17) Pagel, K.; Hyung, S. J.; Ruotolo, B. T.; Robinson, C. V. *Anal. Chem.* **2010**, *82*, 5363.
(18) Beardsley, R. L.; Jones, C. M.; Galhena, A. S.; Wysocki, V. H. *Anal. Chem.* **2009**, *81*, 1347.
(19) Wyttenbach, T.; Bowers, M. T. *Annu. Rev. Phys. Chem.* **2007**, *58*, 511.
(20) Badman, E. R.; Myung, S.; Clemmer, D. E. *J. Am. Soc. Mass Spectrom.* **2005**, *16*, 1493.
(21) Koeniger, S. L.; Merenbloom, S. I.; Clemmer, D. E. *J. Phys. Chem. B* **2006**, *110*, 7017.
(22) van Duijn, E.; Barendregt, A.; Synowsky, S.; Versluis, C.; Heck, A. J. R. *J. Am. Chem. Soc.* **2009**, *131*, 1452.
(23) Hopper, J. T. S.; Oldham, N. J. *J. Am. Soc. Mass Spectrom.* **2009**, *20*, 1851.
(24) Freeke, J.; Robinson, C. V.; Ruotolo, B. T. *Int. J. Mass Spectrom.* **2010**, *298*, 91.
(25) Han, L.; Hyung, S.-J.; Mayers, J. J. S.; Ruotolo, B. T. *J. Am. Chem. Soc.* **2011**, *133*, 11358.
(26) Patriksson, A.; Marklund, E.; van der Spoel, D. *Biochemistry* **2007**, *46*, 933.
(27) Frieman, R.; Larsson, D. S. D.; Wang, Y.; van der Spoel, D. *J. Am. Chem. Soc.* **2009**, *131*, 16606.
(28) Marklund, E.; Larsson, D. S. D.; van der Spoel, D.; Patriksson, A.; Caleman, C. *Phys. Chem. Chem. Phys.* **2009**, *11*, 8069.
(29) Steinberg, M. Z.; Breuker, K.; Elber, R.; Gerber, R. B. *Phys. Chem. Chem. Lett.* **2007**, *9*, 4690.
(30) Thirumuruganandham, S. P.; Urbassek, H. M. *Biochem. Res. Int.* **2010**, *2010*, 213936.
(31) Meyer, T.; de la Cruz, X.; Orozco, M. *Structure* **2009**, *17*, 88.
(32) van der Spoel, D.; Marklund, E.; Larsson, D. S. D.; Caleman, C. *Macromol. Biosci.* **2011**, *11*, 50.
(33) Sun, N.; Soya, N.; Kitova, E. N.; Klassen, J. S. *J. Am. Soc. Mass Spectrom.* **2010**, *21*, 472.
(34) Iavarone, A. T.; Williams, E. R. *J. Am. Chem. Soc.* **2003**, *125*, 2319.
(35) Bush, M. F.; Hall, Z.; Giles, K.; Hoyes, J.; Robinson, C. V.; Ruotolo, B. T. *Anal. Chem.* **2010**, *82*, 9557.
(36) van Der Spoel, D.; Lindahl, E.; Hess, B.; Groenhof, G.; Mark, A. E.; Berendsen, H. J. C. *J. Comput. Chem.* **2005**, *26*, 1701.
(37) Kaminski, G. A.; Friesner, R. A.; Tirado-Rives, J.; Jorgensen, W. L. *J. Phys. Chem. B* **2001**, *105*, 6474.
(38) Hess, B.; Bekker, H.; Berendsen, H. J. C.; Fraaije, J. G. E. M. *J. Comput. Chem.* **1997**, *18*, 1463.
(39) Reimann, C. T.; Valizquez, I.; Tapia, O. *J. Phys. Chem. B* **1998**, *102*, 9344.
(40) Miteva, M.; Demirev, P. A.; Karshikoff, A. D. *J. Phys. Chem. B* **1997**, *101*, 9645.
(41) Schnier, P. D.; Gross, D. S.; Williams, E. R. *J. Am. Soc. Mass Spectrom.* **1995**, *6*, 1086.
(42) Kaltashov, I.; Abzalimov, R. *J. Am. Soc. Mass Spectrom.* **2008**, *19*, 1239.
(43) Chakravarty, S.; Varadarajan, R. *Structure* **1999**, *7*, 723.
(44) Mack, E. *J. Am. Chem. Soc.* **1925**, *47*, 2468.
(45) Mesleh, M. F.; Hunter, J. M.; Shvartsburg, A. A.; Schatz, G. C.; Jarrold, M. F. *J. Phys. Chem.* **1996**, *100*, 16082.
(46) Shvartsburg, A. A.; Jarrold, M. F. *Chem. Phys. Lett.* **1996**, *261*, 86.
(47) Benesch, J. L. P.; Ruotolo, B. T. *Curr. Opin. Struct. Biol.* **2011**, *21*, 641.
(48) Lomeli, S. H.; Peng, I. X.; Yin, S.; Ogorzalek Loo, R. R.; Loo, J. A. *J. Am. Soc. Mass Spectrom.* **2010**, *21*, 127.
(49) Sterling, H. J.; Daly, M. P.; Feld, G. K.; Thoren, K. L.; Kintzer, A. F.; Krantz, B. A.; Williams, E. R. *J. Am. Soc. Mass Spectrom.* **2010**, *21*, 1762.
(50) Lomeli, S. H.; Yin, S.; Ogorzalek Loo, R. R.; Loo, J. A. *J. Am. Soc. Mass Spectrom.* **2009**, *20*, 593.
(51) Fersht, A. R.; Daggett, V. *Cell* **2002**, *108*, 573.
(52) Beck, D. A. C.; Daggett, V. *Methods* **2004**, *34*, 112.
(53) Segev, E.; Wyttenbach, T.; Bowers, M. T.; Gerber, R. B. *Phys. Chem. Chem. Phys.* **2008**, *10*, 3077.
(54) Chen, L.; Shao, Q.; Gao, Y.-Q.; Russell, D. H. *J. Phys. Chem. A* **2011**, *115*, 4427.
(55) Tao, L.; Dahl, D. B.; Perez, L. M.; Russell, D. H. *J. Am. Soc. Mass Spectrom.* **2009**, *20*, 1593.
(56) Knapman, T. W.; Morton, V. L.; Stonehouse, N. J.; Stockley, P. G.; Ashcroft, A. E. *Rapid Commun. Mass Spectrom.* **2010**, *24*, 3033.
(57) Laskowski, R. A. *J. Mol. Graphics* **1995**, *13*, 323.
(58) Bahadur, R.; Zacharias, M. *Cell. Mol. Life Sci.* **2008**, *65*, 1059.
(59) Hubbard, S. J.; Argos, P. *Protein Sci.* **1994**, *3*, 2194.
(60) Bahadur, R. P.; Chakrabarti, P.; Rodier, F.; Janin, J. *Proteins: Struct., Funct., Bioinf.* **2003**, *53*, 708.
(61) Catalina, M. I.; van den Heuvel, R. H. H.; van Duijn, E.; Heck, A. J. R. *Chem.—Eur. J.* **2005**, *11*, 960.
(62) Lemaire, D.; Marie, G.; Serani, L.; Laprevote, O. *Anal. Chem.* **2001**, *73*, 1699.
(63) Hogan, C. J.; Carroll, J. A.; Rohrs, H. W.; Biswas, P.; Gross, M. L. *Anal. Chem.* **2009**, *81*, 369.
(64) Hogan, C. J.; Carroll, J. A.; Rohrs, H. W.; Biswas, P.; Gross, M. L. *J. Am. Chem. Soc.* **2008**, *130*, 6926.
(65) Wanasundara, S. N.; Thachuk, M. *J. Phys.Chem. A* **2009**, *113*, 3814.
(66) Shelimov, K. B.; Clemmer, D. E.; Hudgins, R. R.; Jarrold, M. F. *J. Am. Chem. Soc.* **1997**, *119*, 2240.
(67) van den Heuvel, R. H. H.; van Duijn, E.; Mazon, H.; Synowsky, S. A.; Lorenzen, K.; Versluis, C.; Brouns, S. J. J.; Langridge, D.; van der Oost, J.; Hoyes, J.; Heck, A. J. R. *Anal. Chem.* **2006**, *78*, 7473.
(68) Boeri Erba, E.; Ruotolo, B. T.; Barsky, D.; Robinson, C. V. *Anal. Chem.* **2010**, *82*, 9702.
(69) Blackwell, A. E.; Dodds, E. D.; Bandarian, V.; Wysocki, V. H. *Anal. Chem.* **2011**, *83*, 2862.
(70) Dodds, E. D.; Blackwell, A. E.; Jones, C., M.; Holso, K. L.; O'Brien, D. J.; Cordes, M. H. J.; Wysocki, V. H. *Anal. Chem.* **2011**, *83*, 3881.